VI International Conference on Adaptive Modeling and Simulation
ADMOS 2013
J. P. Moitinho de Almeida, P. Díez, C. Tiago and N. Parés (Eds)

NON-CONFORMING FINITE ELEMENT METHODS FOR THE OBSTACLE PROBLEM

C. Carstensen[*,†] **and K. Köhler**[*]

[*]Institut für Mathematik, Humboldt-Universität zu Berlin, Unter den Linden 6, D-10099 Berlin, Germany

[†]Department of CSE, Yonsei University, Seoul, Korea

Key words: obstacle problem, a priori error estimate, a posteriori error estimate, efficiency

Abstract. In an obstacle problems with an affine obstacle, homogeneous Dirichlet boundary conditions, and standard regularity assumptions, the Crouzeix-Raviart non-conforming finite element method (FEM) allows for linear convergence as the maximal mesh-size approaches zero. The residual-based a posteriori error analysis leads to reliable and efficient control over the error with explicit constants. It involves the design of a new discrete Lagrange multiplier and allows for the computation of a guaranteed upper error bound. A novel energy control for non-conforming FEMs lead to a computable guaranteed lower bound for the minimal energy. The paper presents numerical experiments to investigate the theoretical results empirically and so to explore the possibilities of the non-conforming finite element method with respect to adaptive mesh refinement in practice.

1 INTRODUCTION

Given a bounded polygonal Lipschitz domain $\Omega \subset \mathbb{R}^2$ with boundary $\partial\Omega$, the energy product $a : H^1(\Omega) \times H^1(\Omega) \to \mathbb{R}$ on the Hilbert space $H^1(\Omega)$ reads

$$a(u, v) = \int_\Omega \nabla u \cdot \nabla v dx \quad \text{for all } u, v \in H^1(\Omega)$$

and induces the energy semi-norm $|||\cdot||| := a(\cdot, \cdot)^{1/2}$, which is a norm on the vector space $V := H^1_0(\Omega) := \{v \in H^1(\Omega) | \, v = 0 \text{ on } \partial\Omega\}$. Given some source term $f \in L^2(\Omega)$ set $F \in L^2(\Omega)^*$ by

$$F(v) := \int_\Omega f v dx \quad \text{for all } v \in L^2(\Omega).$$

The obstacle $\chi \in H^2(\Omega) \cap W^{1,\infty}(\Omega)$ satisfies $\chi \leq 0$ along $\partial\Omega$ in order to ensure that the closed and convex subset

$$K := \{v \in H^1_0(\Omega) \mid \chi \leq v \text{ a.e.}\} \quad \text{of } H^1_0(\Omega)$$

is non-empty. The well established weak formulation of the obstacle problem seeks $u \in K$ such that

$$F(v-u) \leq a(u, v-u) \quad \text{for all } v \in K. \tag{1.1}$$

It is well known [KS80], that a unique weak solution u of (1.1) exists. The a priori convergence analysis of [Fal74] provides linear convergence of the error in the H^1 semi-norm $|||\bullet|||$ for $u \in H^2(\Omega)$ approximated by a P_1 conforming finite element method. The more recent analysis of [Wan03] for a non-conforming P_1 FEM requires $u \in W^{s,p}(\Omega)$ for some $2 < p$ and $2 < s < 2 + 1/p$.

The non-conforming finite element method seeks some approximation in the set K_{NC} where the obstacle condition is tested at the midpoints of the edges in a regular triangulation of the polygonal domain into triangles. Hence the term non-conforming refers to the fact that the discrete solution is not a Sobolev function as well as to the additional fact that the discrete solution u_{CR} does not satisfy the obstacle condition almost everywhere in the domain.

This paper announces some theoretical results which guarantee linear convergence for the error in the discrete energy norm for any weak solution u in $H^2(\Omega)$ which is in parallel analogy to the classical result [Fal74] for conforming FEMs. The adaptive mesh-refinement is based on some a posteriori analysis and the first reliable and efficient error estimators are introduced and tested in this paper; cf. [BC04], [Vee01], [CM10], and [Bra05] for conforming first-order methods. Three computational benchmarks are revisited to empirically verify the theoretical predictions. The aim is to provide numerical evidence for the guaranteed error control and for the superiority of adaptive over uniform mesh-refinements.

The rather technical proofs for the underlying theoretical statements utilise the medius analysis in that they combine arguments from the a priori and a posteriori error analysis and will appear elsewhere.

The remaining parts of this paper are organised as follows. Section 2 introduces the discretisation of the obstacle problem. Section 3 presents a new a priori error analysis under minimal regularity assumptions and an a posteriori error result. The paper concerns three computational benchmark examples in Section 4. The first example discusses a typical corner singularity on an L-shaped domain. The second concerns a smooth obstacle on a square domain and the third has a piecewise affine obstacle also on a square domain.

Throughout this paper, the standard notation for Lebesgue and Sobolev spaces and their norms $\|\bullet\|_{L^2(\Omega)}$, $|||\bullet||| = \|\nabla\bullet\|_{L^2(\Omega)}$ and $|||\bullet|||_{\mathrm{NC}} := \|\nabla_{NC}\bullet\|_{L^2(\Omega)}$ and their local variants are used. Moreover $A \lesssim B$ abbreviates $A \leq CB$ for some generic constant C and $A \approx B$ abbreviates $A \lesssim B \lesssim A$.

2 Preliminaries

2.1 Discretisation

Let $\Omega \subset \mathbb{R}^2$ be a bounded polygonal Lipschitz domain partitioned in a shape-regular triangulation $\mathcal{T}$ into triangles with the set of edges $\mathcal{E}$ and interior edges $\mathcal{E}(\Omega)$. Any edge $E \in \mathcal{E}$ has length $|E|$, the midpoint $\mathrm{mid}(E)$, the unit normal ν_E and the tangent τ_E; $\mathrm{mid}(\mathcal{E}) := \{\mathrm{mid}(E)|\ E \in \mathcal{E}\}$ denotes the set of all midpoints. The subdivision of each triangle $T \in \mathcal{T}$ into four congruent

sub-triangles by straight lines through the edges midpoints results in the red-refined triangulation $red(\mathcal{T})$. For any $k \in \mathbb{N}_0$, set

$$\begin{aligned}
P_k(T) &:= \{v_k : T \to \mathbb{R} |\ v_k \text{ is a polynomial of degree} \leq k\},\\
P_k(\mathcal{T}) &:= \{v_k \in L^2(\Omega) |\ \forall T \in \mathcal{T},\ v_k|_T \in P_k(T)\},\\
\mathrm{CR}^1(\mathcal{T}) &:= \{v_{\mathrm{CR}} \in P_1(T) |\ v_{\mathrm{CR}} \text{ continuous at } \mathrm{mid}(\mathcal{E})\},\\
\mathrm{CR}^1_0(\mathcal{T}) &:= \{v_{\mathrm{CR}} \in \mathrm{CR}^1(\mathcal{T}) |\ \forall E \in \mathcal{E}(\partial\Omega),\ v_{\mathrm{CR}}(\mathrm{mid}(E)) = 0\},\\
\mathrm{K}_{\mathrm{NC}} &:= \{v_{\mathrm{CR}} \in \mathrm{CR}^1_0(\mathcal{T}) |\ \forall E \in \mathcal{E}(\Omega),\ \fint_E \chi ds \leq v_{\mathrm{CR}}(\mathrm{mid}(E))\}.
\end{aligned}$$

The triangulation $\mathcal{T}$ is shape regular in the sense that any interior angle of any triangle is bounded from below by some universal positive constant ω_0 and all the generic constants hidden in the notation $\lesssim$ may depend on $\omega_0 > 0$. The triangulation $\mathcal{T}$ is regular in the sense that any two distinct triangles in $\mathcal{T}$ with non-empty intersection are either identical or share exactly one common node or one common edge. For any triangulation $\mathcal{T}$, define the (local) mesh-size $h_{\mathcal{T}} \in P_0(\mathcal{T})$ and L^2-projection $\Pi_0 : L^2(\Omega) \to P_0(\Omega)$ by $h_{\mathcal{T}}|_T := h_T := diam(T)$ and $\Pi_0|_T f := \fint_T f dx$ for all $T \in \mathcal{T}$ and $f \in L^2(\Omega)$, with the integral mean $\fint_T \bullet\, dx := \int_T \bullet\, dx/|T|$. With the piecewise gradient $\nabla_{\mathrm{NC}} v_{\mathrm{CR}}$ of any discrete function $v_{\mathrm{CR}} \in \mathrm{CR}^1(\mathcal{T})$, the discrete energy product $a_{\mathrm{NC}} : \mathrm{CR}^1(\mathcal{T}) \times \mathrm{CR}^1(\mathcal{T}) \to \mathbb{R}$ reads

$$a_{\mathrm{NC}}(u_{\mathrm{CR}}, v_{\mathrm{CR}}) := \int_\Omega \nabla_{\mathrm{NC}} u_{\mathrm{CR}} \cdot \nabla_{\mathrm{NC}} v_{\mathrm{CR}} dx \quad \text{for all } u_{\mathrm{CR}}, v_{\mathrm{CR}} \in \mathrm{CR}^1(\mathcal{T})$$

and induces the discrete energy semi-norm $|||\cdot|||_{\mathrm{NC}} := a_{\mathrm{NC}}(\cdot,\cdot)^{1/2}$ in $\mathrm{CR}^1(\mathcal{T})$. Owing to the discrete Friedrichs inequality $\|v_{\mathrm{CR}}\|_{L^2(\Omega)} \lesssim |||v_{\mathrm{CR}}|||_{\mathrm{NC}}$ for all $v_{\mathrm{CR}} \in \mathrm{CR}^1(\mathcal{T})$ (cf. [BS08]) this is a norm in $\mathrm{CR}^1_0(\mathcal{T})$.
The discrete analogue to the variational inequality (1.1) seeks $u_{\mathrm{CR}} \in \mathrm{K}_{\mathrm{NC}}$ with

$$F(v_{\mathrm{CR}} - u_{\mathrm{CR}}) \leq a_{\mathrm{NC}}(u_{\mathrm{CR}}, v_{\mathrm{CR}} - u_{\mathrm{CR}}) \quad \text{for all } v_{\mathrm{CR}} \in \mathrm{K}_{\mathrm{NC}}\,. \tag{2.1}$$

The abstract results on variational inequalities in the Hilbert space $\left(\mathrm{CR}^1(\mathcal{T}), a_{\mathrm{NC}}\right)$ guarantee the unique existence of a discrete solution u_{CR}. Each edge $E \in \mathcal{E}(\Omega)$ is associated with its edge-oriented basis function $\psi_E \in \mathrm{CR}^1(\mathcal{T})$ such that $\psi_E \equiv 1$ along E while $\psi_E(\mathrm{mid}(F)) = 0$ for any other edge $F \in \mathcal{E}\backslash\{E\}$, and its support $\overline{\omega_E} := \cup\{T \in \mathcal{T} |\ E \in \mathcal{E}(T)\}$. For each edge $E \in \mathcal{E}(\Omega)$, the solution u_{CR} to the discrete variational inequality (2.1) satisfies the discrete consistency condition

$$0 \leq u_{\mathrm{CR}}(\mathrm{mid}(E)) - \fint_E \chi ds \perp F(\psi_E) - a_{\mathrm{NC}}(u_{\mathrm{CR}}, \psi_E) \leq 0. \tag{2.2}$$

This follows from direct considerations with the degrees of freedom in (2.1) and is the discrete analogue of the well known (continuous) consistency condition [KS80] for $u \in H^2_{loc}(\Omega)$ which satisfies

$$0 \leq u - \chi \perp f + \Delta u \leq 0 \quad \text{almost everywhere in } \Omega. \tag{2.3}$$

3 Error Analysis

This section provides an a priori and a posteriori error estimate for the error $|||u - u_{\mathrm{CR}}|||_{\mathrm{NC}}$ for the solutions u and u_{CR} of the continuous and discrete obstacle problem (1.1) and (2.1) as well as lower bounds of the minimal energy $E(u)$ based on the discrete energy $E_{NC}(u_{\mathrm{CR}})$.

Theorem 3.1 (a priori error estimate) *The continuous and discrete solutions $u \in K$ and $u_{\mathrm{CR}} \in \mathrm{K}_{\mathrm{NC}}$ to the obstacle problem with $u \in H^2(\Omega)$ satisfy*

$$|||u - u_{\mathrm{CR}}|||_{\mathrm{NC}} \lesssim \|h_{\mathcal{T}} f\|_{L^2(\Omega)} + \left\|h_{\mathcal{T}} D^2 u\right\|_{L^2(\Omega)} + \|\chi - \mathrm{I}_{\mathrm{NC}}\chi\|_{L^\infty(\Omega)} + \|h_{\mathcal{T}} \nabla(\chi - \mathrm{I}_{\mathrm{NC}}\chi)\|_{L^\infty(T)}\,. \qquad \square$$

Given the discrete Crouzeix-Raviart solution $u_{\mathrm{CR}} \in K_{NC}$, define some function

$$\lambda_{CR} := \sum_{E \in \mathcal{E}(\Omega)} \rho_E \frac{\psi_E}{\|\psi_E\|^2_{L^2(\Omega)}} \text{ with } \rho_E := F(\psi_E) - a_{\mathrm{NC}}(u_{\mathrm{CR}}, \psi_E) \tag{3.1}$$

for the edge-oriented basis function $\psi_E \in \mathrm{CR}^1(\mathcal{T})$ associated to the edge $E \in \mathcal{E}(\Omega)$. It holds

$$\Lambda_{CR}(v_{\mathrm{CR}}) = \int_\Omega \lambda_{CR} v_{\mathrm{CR}} dx \text{ for all } v_{\mathrm{CR}} \in \mathrm{CR}^1_0(\mathcal{T}).$$

In the sequel, $\Lambda_{CR}(v)$ always denotes the L^2 scalar product of any Lebesgue function $v \in L^2(\Omega)$ with the above $\lambda_{CR} \in \mathrm{CR}^1_0(\mathcal{T})$. The following a posteriori error estimate involves the continuous Lagrange multiplier

$$\Lambda := F - a(u, \bullet) \in V^*$$

with the L^2 representation $\lambda = f + \Delta u$. Define $|||\Lambda - \Lambda_{CR}|||_*$ by

$$|||\Lambda - \Lambda_{CR}|||_* := \sup_{v \in V \setminus \{0\}} \int_\Omega (\lambda - \lambda_{CR})(v) dx / |||v|||.$$

Theorems 3.2-3.3 utilise the subset $\mathcal{T}' := \left\{T \in \mathcal{T} \;\middle|\; 0 < |\{x \in T | \lambda_{CR}(x) > 0\}|\right\}$ of $\mathcal{T}$ with the 2D Lebesgue measure $|\bullet|$ and the oscillations of a function g given by

$$\mathrm{osc}(g, \mathcal{T}) := \sqrt{\sum_{T \in \mathcal{T}} h_T^2 \|g - \Pi_0 g\|^2_{L^2(T)}}.$$

Theorem 3.2 (guaranteed upper error bound) *Any $v \in K$ satisfies*

$$\begin{aligned}
&\text{ⓐ } 1/2 |||u - u_{\mathrm{CR}}|||^2_{\mathrm{NC}} + \Lambda(u - v) + \int_{\mathcal{T}'} (\chi - u)\Pi_0 \lambda_{CR} dx + \int_{\mathcal{T} \setminus \mathcal{T}'} (\chi - u) \lambda_{CR} dx \\
&\quad \le 1/2 \left(\kappa_{CR} \|h_{\mathcal{T}}(f - \lambda_{CR})\|_{L^2(\Omega)} + \mathrm{osc}(\lambda_{CR}, \mathcal{T}')/j_{1,1}\right)^2 + 1/2 |||v - u_{\mathrm{CR}}|||^2_{\mathrm{NC}} \\
&\qquad + \int_{\mathcal{T}'} (\chi - v)\Pi_0 \lambda_{CR} dx + \int_{\mathcal{T} \setminus \mathcal{T}'} (u_{\mathrm{CR}} - v) \lambda_{CR} dx; \\
&\text{ⓑ } |||\Lambda - \Lambda_{CR}|||_* \le |||u - u_{\mathrm{CR}}|||_{\mathrm{NC}} + \mathrm{osc}(f - \lambda_{CR}, \mathcal{T})/j_{1,1} \\
&\qquad + 1/2 \|\Pi_0(f - \lambda_{CR})(\bullet - \mathrm{mid}(\mathcal{T}))\|_{L^2(\Omega)} + |||u_{\mathrm{CR}} - v|||_{\mathrm{NC}}. \qquad \square
\end{aligned}$$

The universal constant $\kappa_{CR} \leq 0.298217419$ is derived from an interpolation error estimate for the non-conforming interpolant $\mathrm{I_{NC}}$ as in [CGR12]. The lower bound for the exact energy $E(u)$ is given in the following theorem.

Theorem 3.3 (lower bound for the minimal energy) *The discrete solution u_{CR} and the continuous solution u to the obstacle problem satisfy*

$$\begin{aligned}
&ⓐ\ E_{NC}(u_{\mathrm{CR}}) - \frac{\kappa_{CR}^2}{2}\,\|h_{\mathcal{T}} f\|^2_{L^2(\Omega)} \leq E(u);\\
&ⓑ\ E_{NC}(u_{\mathrm{CR}}) - \left(\kappa_{CR}\,\|h_{\mathcal{T}}(f-\lambda_{CR})\|_{L^2(\Omega)} + \mathrm{osc}(\lambda_{CR},\mathcal{T}')\right)^2/2\\
&\quad - \int_{\mathcal{T}'}(\chi - u_{\mathrm{CR}})\Pi_0\lambda_{CR}dx + \int_{\mathcal{T}\setminus\mathcal{T}'}(\mathrm{I_{NC}}\chi - \chi)\lambda_{CR}dx \leq E(u).
\end{aligned}$$ □

For any $v \in K$, the a posteriori error estimate of Theorem 3.2 leads to a computable global upper bound $GUB(v)$ of the five non-negative error terms in $LHS(v)$

$$\begin{aligned}
LHS(v) :=& |||u - u_{\mathrm{CR}}|||_{\mathrm{NC}} + \Lambda(u-v)^{1/2} + \left(\int_{\mathcal{T}'}\lambda_{CR}\Pi_0(\chi - u)dx\right)^{1/2}\\
&+ \left(\int_{\mathcal{T}\setminus\mathcal{T}'}(\mathrm{I_{NC}}\chi - u)\lambda_{CR}dx\right)^{1/2} + |||\Lambda - \Lambda_{CR}|||_* \lesssim GUB(v)\\
GUB(v) :=& \|h_{\mathcal{T}}(f-\lambda_{CR})\|_{L^2(\Omega)} + \mathrm{osc}(\lambda_{CR},\mathcal{T}') + |||v - u_{\mathrm{CR}}|||_{\mathrm{NC}}\\
&+ \left(\int_{\mathcal{T}'}\lambda_{CR}\Pi_0(\chi - v)dx\right)^{1/2} + \left(\int_{\mathcal{T}\setminus\mathcal{T}'}\lambda_{CR}(u_{\mathrm{CR}} - v)dx\right)^{1/2}\\
&+ \mathrm{osc}(f-\lambda_{CR},\mathcal{T}) + \|\Pi_0(f-\lambda_{CR})(\bullet - \mathrm{mid}(\mathcal{T}))\|_{L^2(\Omega)}.
\end{aligned}$$

This reliable error bound is efficient in the sense that the converse inequality holds up to some generic factor hidden in the notation $\lesssim$ and up to data oscillations.

Theorem 3.4 (efficiency) *Any function $v \in K$ with $|||u - v||| \lesssim |||u - u_{\mathrm{CR}}|||_{\mathrm{NC}}$ satisfies*

$$GUB(v) \lesssim LHS(v) + \mathrm{osc}(f,\mathcal{T}) + \mathrm{osc}(\lambda,\mathcal{T}).$$ □

4 Computational Benchmarks

This section is devoted to the presentation of a novel adaptive mesh-refinement algorithm and the empirical investigation of the superiority of adaptive over uniform meshes, the computational comparison of conforming and non-conforming first-order FEMs and the verification of the guaranteed error and energy bounds in practice.

4.1 Numerical Realisation

Adaptive Algorithm. INPUT is a coarse mesh $\mathcal{T}_0$, and a parameter $0 < \theta \leq 1$.
LOOP For level $\ell = 0, 1, 2, ...$ until termination do

COMPUTE the discrete solution u_{CR} on $\mathcal{T}_\ell$ with `ndof` many unknowns with code similar to [ACF].
ESTIMATE the error $|||u - u_{\mathrm{CR}}|||^2_{\mathrm{NC}}$ with any of the estimators $\eta_{P1red}, \eta_{Energy}, \eta_{J2}$ defined below.
Theorem 3.2 leads to an estimator

$$\eta_v^2(T) := \Big(\kappa_{CR}\,\|h_{\mathcal{T}}(f-\lambda_{CR})\|_{L^2(T)} + Osc(\lambda_{CR},T)/j_{1,1}\Big)^2 + |||v-u_{\mathrm{CR}}|||^2_{\mathrm{NC}(T)} + 2I(T)$$

where

$$Osc(\lambda_{CR},T) := \begin{cases} osc(\lambda_{CR},T) \text{ for } T\in\mathcal{T}', \\ 0 \text{ for } T\in\mathcal{T}\setminus\mathcal{T}', \end{cases} \qquad I(T) := \begin{cases} \int_{T'}(\chi - v)\Pi_0\lambda_{CR}dx \text{ for } T\in\mathcal{T}', \\ \int_{T'}(u_{\mathrm{CR}} - v)\lambda_{CR}dx \text{ for } T\in\mathcal{T}\setminus\mathcal{T}'. \end{cases}$$

The estimator depends on a function $v \in K$. Three different possibilities ⓐ – ⓒ for $v \in P_1(red(\mathcal{T}))\cap C_0(\Omega)\cap K$ are presented in this paper all of which follow from linear interpolation once the values at the nodes are defined.
ⓐ v_{P1red} is computed in two steps. In a first step a function w_2 is defined to equal $u_{\mathrm{CR}}(mid(\mathcal{E}))$ at the edges' midpoints and the values at a node $z\in\mathcal{N}(\Omega)$ are chosen such that on the patch ω_z^* w_2 minimises $1/2|||w-u_{\mathrm{CR}}|||^2_{\mathrm{NC}(\omega_z^*)} + \int_{\omega_z^*}(\chi - w)\Pi_0\lambda_{CR}dx + \int_{\omega_z^*}(u_{\mathrm{CR}}-w)\lambda_{CR}dx$ over all function $w\in P_1(red(\mathcal{T}))\cap C_0(\Omega)$. This is a one dimensional minimisation problem. In a second step set $v := P_K(w_2)$ where P_K is the projection onto the set of admissible function with respect to the energy norm.
ⓑ v_{Energy} is computed in two steps. In a first step a function w_2 is defined which equals $u_{\mathrm{CR}}(mid(\mathcal{E}))$ at the edges' midpoints and the values at a node $z\in\mathcal{N}(\Omega)$ are chosen such that on the patch ω_z^* w_2 minimises $E(w) - E_{NC}(u_{\mathrm{CR}})$ locally over all function $w\in P_1(red(\mathcal{T}))\cap C_0(\Omega)$. This is a one dimensional minimisation problem. In a second step set $v := P_K(w_2)$ where P_K is the projection onto the set of admissible function with respect to the energy norm.
ⓒ v_{J2} is set to the arithmetic mean of the different values of u_{CR} at the nodes. The values at the edges' midpoints are chosen such that $\fint_E v_{J2}\,ds = u_{\mathrm{CR}}(\mathrm{mid}(E))$ along any edge $E\in\mathcal{E}$.
Those three functions lead to the error estimators $\eta_{P1red}, \eta_{Energy}, \eta_{J2}$.
With Theorem 3.3 estimate the lower bounds μ_j, $(j=1,2)$ for the energy defined as

$$\begin{aligned}\mu_1 :=& E_{NC}(u_{\mathrm{CR}}) - \frac{\kappa_{CR}^2}{2}\,\|h_{\mathcal{T}}f\|^2_{L^2(\Omega)} \\ \mu_2 :=& E_{NC}(u_{\mathrm{CR}}) - \Big(\kappa_{CR}\,\|h_{\mathcal{T}}(f-\lambda_{CR})\|_{L^2(\Omega)} + \mathrm{osc}(\lambda_{CR},\mathcal{T}')\Big)^2/2 \\ &- \int_{\mathcal{T}'}(\chi - u_{\mathrm{CR}})\Pi_0\lambda_{CR}dx + \int_{\mathcal{T}\setminus\mathcal{T}'}(\mathrm{I}_{\mathrm{NC}}\chi - \chi)\lambda_{CR}dx.\end{aligned}$$

MARK the minimal set $\mathcal{M}_\ell\subseteq\mathcal{T}_\ell$ such that

$$\theta\sum_{T\in\mathcal{T}_\ell}\eta(T) \le \sum_{T\in\mathcal{M}_\ell}\eta(T).$$

REFINE by red-refinement of elements in $\mathcal{M}_\ell$ and red-green-blue-refinement of further elements to avoid hanging nodes and compute $\mathcal{T}_{\ell+1}$. od
OUTPUT efficiency indices $\sqrt{\sum_{T\in\mathcal{T}}\eta_v^2(T)}/|||u-u_{\mathrm{CR}}|||_{\mathrm{NC}}$.

4.2 L-Shaped Domain

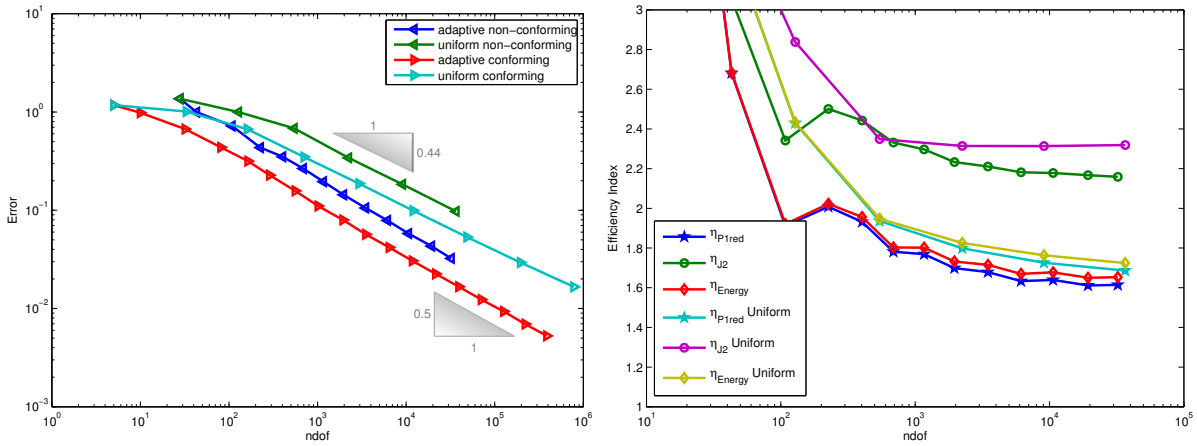

Figure 4.1: Convergence history of the exact errors for the non-conforming and conforming FEM on uniform and adaptive meshes (left) and efficiency indices (right) of the three different error estimators for the non-conforming scheme as functions of the number of unknowns on adaptive and uniform meshes for the Example 1 with the error estimators from Theorem 3.2.

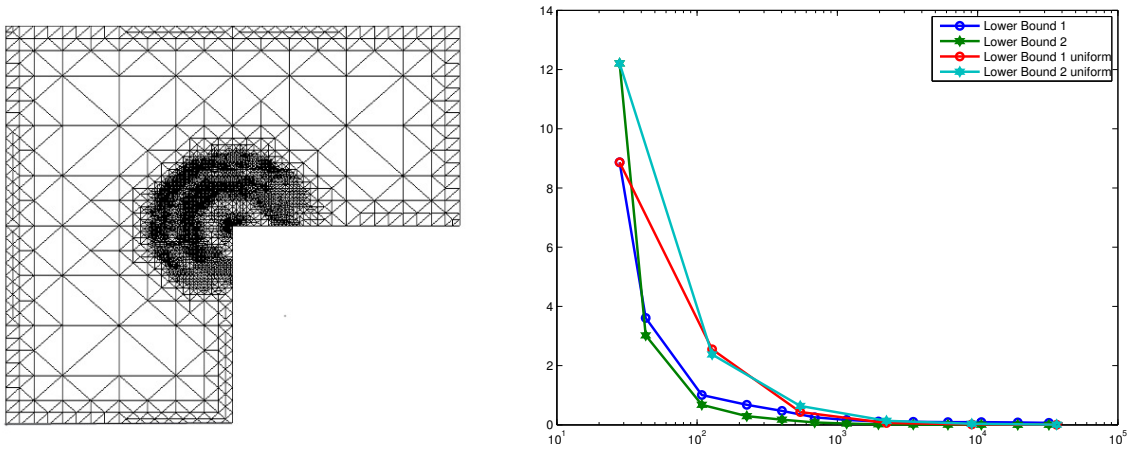

Figure 4.2: Adaptive mesh with refinement indicator η_{P1red} (left) and $E(u)-$lower bound for the lower bounds μ_1 and μ_2 of the exact energy $E(u)$ on uniform and adaptive meshes for Example 1.

The first example from [BC04] involves the L-shaped domain $\Omega := (-2,\ 2)^2\backslash([0,\ 2] \times [-2,\ 0])$, the obstacle $\chi := 0$, the Dirichlet data $u_D := 0$, and the source term

$$f(r,\varphi) := -r^{2/3} sin(2\varphi/3)(7/3(\partial g/\partial r)(r)/r + (\partial^2 g/\partial r^2)(r)) - H(r-5/4)$$
$$g(r) := \max\{0, \min\{1, -6s^2 + 15s^4 - 10s^3 + 1\}\} \text{ for } s := 2(r-1/4)$$

with the Heaviside function H. The exact singular solution reads

$$u(r,\varphi) = r^{2/3} g(r) \sin(2\varphi/3)$$

and has a typical corner singularity at the re-entrant corner. The experiments on uniform meshes show an experimental convergence rate of approximately -0.44 in terms of the number of degrees of freedom which appears suboptimal when compared with the optimal rate $-1/2$ for linear convergence for the conforming and the non-conforming finite element method. The non-conforming FEM leads to efficiency indices between 1.6 and 3 as shown in Figure 4.1 on the right. For the calculation of the efficiency index it needs to be taken into account, that the error estimator does not only estimate $|||u - u_{\mathrm{CR}}|||_{\mathrm{NC}}$ but also the terms

$$|||u - u_{\mathrm{CR}}|||_{\mathrm{NC}} + \Lambda(u - v)^{1/2} + \left(\int_{\mathcal{T}'} \lambda_{CR} \Pi_0(\chi - u) dx \right)^{1/2} + \left(\int_{\mathcal{T} \setminus \mathcal{T}'} (\mathrm{I}_{\mathrm{NC}} \chi - u) \lambda_{CR} dx \right)^{1/2} + |||\Lambda - \Lambda_{CR}|||.$$

The computation of the entire exact error will lead to even better efficiency indices. The adaptive algorithm for the non-conforming method, with η_{P1red} as the refinement indicator, leads to an improved convergence rate of approximately -0.5. An adaptive algorithm for the conforming scheme shows the same behaviour (see Figure 4.1 on the left). This indicates, that the error estimators yield good results on unstructured grids as well as on uniformly refined meshes. The efficiency indices for the non-conforming method on an adaptive mesh are comparable to the efficiency indices on uniform meshes (see Figure 4.1). Furthermore the mesh displayed in Figure 4.2 (left) shows, that the contact zone is less refined by the refinement indicator η_{P1red} then the area around the re-entering corner at the point $(0, 0)$, although the boundary of the contact zone is well refined and clearly visible. The lower bounds for the minimal energy $E(u)$ show very similar behaviour. Both lower bounds converge slightly faster for the adaptive algorithm with η_{P1red} as a refinement indicator, than on uniform meshes as demonstrated in Figure 4.2 on the right.

4.3 Smooth Obstacle

This example from [GK09] on the square domain $\Omega := (-1,\ 1)^2$ involves the smooth obstacle $\chi(x, y) := -(x^2 - 1)(y^2 - 1)$, the homogeneous Dirichlet data $u_D|_{\partial\Omega} := 0$ and the source term $f := \Delta\chi$. The exact solution to this problem reads $u = \chi$. On uniformly refined meshes both the conforming and non-conforming finite element method lead to an experimental convergence rate of -0.5. Both methods converge with the same convergence rate for an adaptively refined mesh; cf. Figure 4.3 on the left. The non-conforming scheme leads to good efficiency indices. Again it needs to be taken into account, that more terms of the exact error are estimated. Figure 4.3 right shows the efficiency indices both for a uniform mesh and an adaptive mesh. For this example the adaptive algorithm leads to an almost uniform refinement of the entire domain,

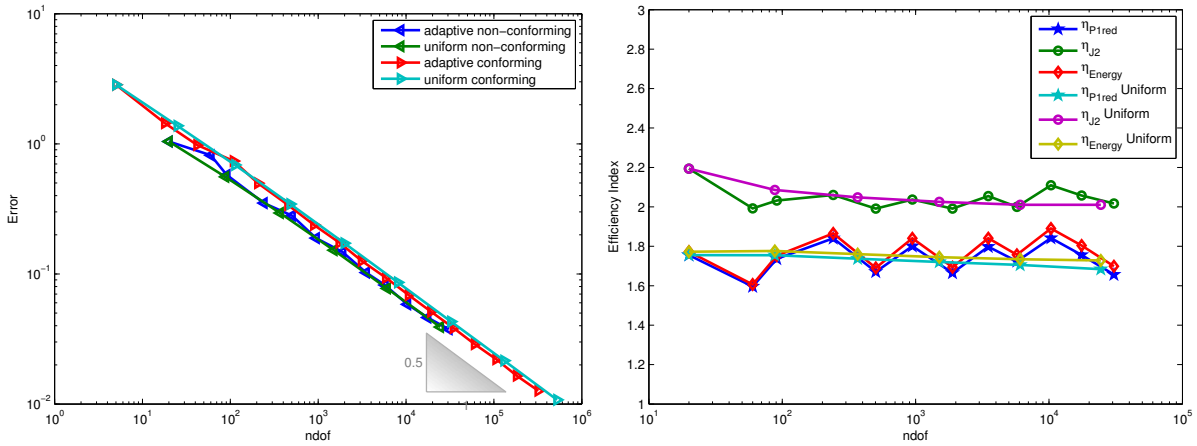

Figure 4.3: Convergence history of the exact errors for the non-conforming and conforming FEM on uniform and adaptive meshes (left) and efficiency indices (right) of the three different error estimators for the non-conforming scheme as functions of the number of unknowns on adaptive and uniform meshes for the Example 2 with the error estimators from Theorem 3.2.

although the central part and the corners are refined more strongly as can be seen in Figure 4.4 on the left. The adaptive refinement does not indicate the contact zone for this problem. The lower bounds for the minimal energy are comparable for this example as well. They converge with a very similar behaviour both on uniform meshes and on an adaptively refined mesh with the refinement indicator η_{P1red} although the adaptive algorithm leads to slightly better results (see Figure 4.4 on the right).

4.4 Pyramid Problem

This example from [BC04] has an unknown exact solution u. The experiment is conducted on the square domain $\Omega := (-1,\ 1)^2$ and involves the pyramidal obstacle $\chi(x, y) := \text{dist}(x, y, \partial\Omega)$. This experiment has homogeneous Dirichlet data and the constant source term $f := 1$. The exact solution is approximated by solving the discrete problem after two additional red refinements in each step. Both the conforming and the non-conforming scheme lead to the experimental convergence rate of -0.5 on uniform meshes, as can be seen in Figure 4.5 on the right. The adaptive algorithm does not show this convergence rate but rather has very bad convergence. On uniform meshes additional undocumented experiments show that the error estimator for the non-conforming finite element method only converge with a convergence rate of -0.3. The efficiency indices in Figure 4.5 on the right confirm this, as they do not tend to a constant value but continue to rise. This does not contradict Theorem 3.2 as the error estimate is still reliable. The efficiency in Theorem 3.4 is shown for all the error term $|||u - u_{\text{CR}}|||_{\text{NC}} + |||\Lambda - \Lambda_{CR}|||_* + \Lambda(u - v) + \int_\Omega \lambda_{CR}\Pi_0(\chi - u)dx$. The numerical experiments only considers the error term $|||u - u_{\text{CR}}|||_{\text{NC}}$ and hence indicate that the remaining terms have more impact on the overall error then in the other examples. Furthermore, the approximation of u by two additional red refinements might not be a good approximation and can lead to errors. The mesh created by the adaptive algorithm

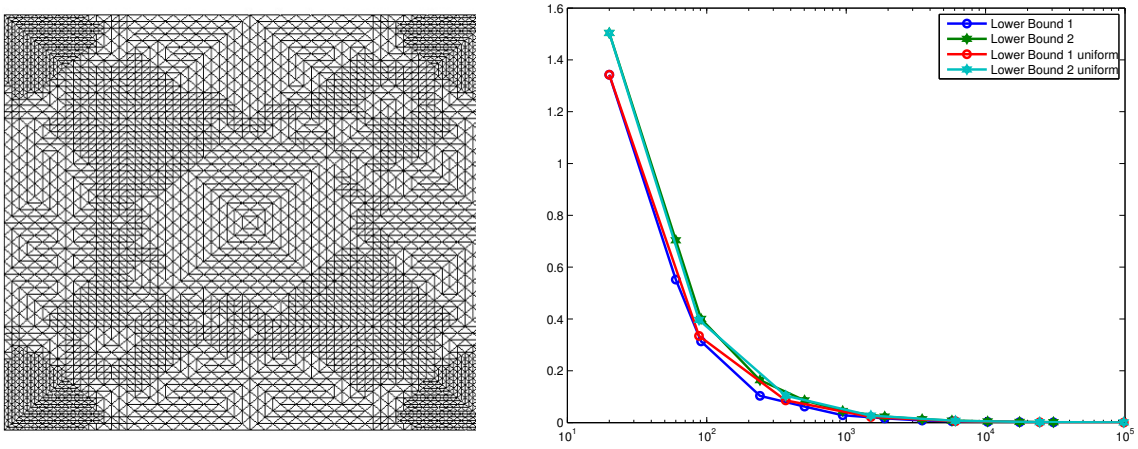

Figure 4.4: Adaptive mesh with refinement indicator η_{P1red} (left) and $E(u)-$lower bound for the lower bounds μ_1 and μ_2 of the exact energy $E(u)$ on uniform and adaptive meshes for Example 2.

depicted in Figure 4.6 on the left demonstrates very clearly the one-dimensional contact zone, which is the union of the two diagonals. The area towards the diagonals is much more refined. Figure 4.6 on the right shows the quality of the lower bounds of the exact energy. As in the examples before the lower bound μ_1 shows the better convergence. This holds true, both for the adaptive algorithm with the refinement indicator η_{P1red} and for the calculation on uniform meshes. In this example the initial mesh is aligned with the obstacle and hence it does not make a big difference whether the adaptive or the uniform mesh design is employed.

5 Conclusions

The numerical experiments confirm the theoretical results from Section 3. It is clearly shown that guaranteed upper error bounds are possible even for a non-conforming discretisation of the non-linear obstacle problem. The accuracy of the non-conforming method differs from those of the conforming scheme only by a multiplicative constant, but overall they show the same convergence rate in terms of the number of degrees of freedom. This is in contrast to the statement on page 111 in [Bra07]: In the numerical experiments of this paper, even for a singular solution, the convergence rate is comparable for conforming and non-conforming FEMs; cf. [CPS12] and the website [Bra].

The first two benchmark examples show that an adaptive algorithm leads to the optimal convergence rate of -0.5 whereas, in Example 1, the uniform algorithm only leads to a convergence rate of -0.44. The third benchmark example does not show this improved behaviour with respect to the convergence rate but, nonetheless, the adaptive algorithm leads to an improvement of the efficiency indices. For uniform refinement the error control for this example is not efficient, but this proves to be the case for adaptive refinement.

The lower bounds of the minimal energy show that the bound μ_1 is preferable to the lower

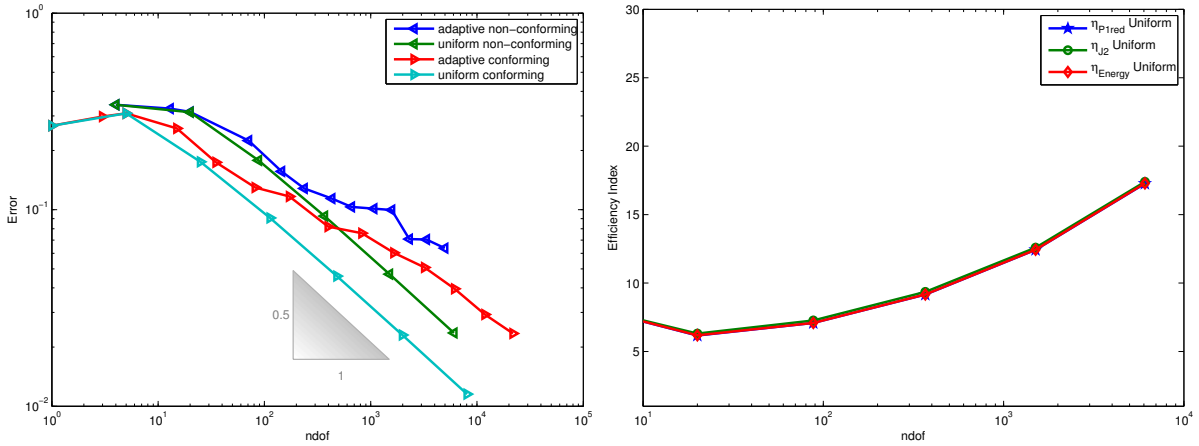

Figure 4.5: Convergence history of the exact errors for the non-conforming and conforming FEM on uniform and adaptive meshes (left) and efficiency indices (right) of the three different error estimators for the non-conforming scheme as functions of the number of unknowns on adaptive and uniform meshes for the Example 3 with the error estimators from Theorem 3.2.

bound μ_2, although in the examples at hand, the difference between the two estimates, as well as between uniform and adaptive mesh refinement is marginal. All three experiments conducted for this paper show that an adaptively refined mesh also leads to better lower bounds for the energies.

All the adaptive refinements were done with the error estimator η_{P1red} as a refinement indicator. Undocumented experiments show that the same adaptive algorithm with either η_{J2} or η_{Energy} as refinement indicators establish comparable results.

Acknowledgements

The results of the conforming FEM were kindly provided by Christian Merdon.

REFERENCES

[ACF] J. Alberty, C. Carstensen, and S.A. Funken. Remarks aroung 50 lines of matlab: short finite element implementation. *Numerical Algorithms*, 20.

[BC04] S. Bartels and C. Carstensen. Averaging techniques yield reliable a posteriori finite element error control for obstacle problems. *Numer. Math*, 99(2):225–249, 2004.

[Bra] D. Braess. Finite elements. theory, fast solvers and applications in solid mechanics. http://homepage.ruhr-uni-bochum.de/dietrich.braess/FEM_corr_eng3.htm.

[Bra05] Dietrich Braess. A posteriori error estimators for obstacle problems—another look. *Numer. Math.*, 101(3), 2005.

[Bra07] Dietrich Braess. *Finite elements: Theory, fast solvers, and applications in solid mechanics*. Cambridge University Press, 2007.

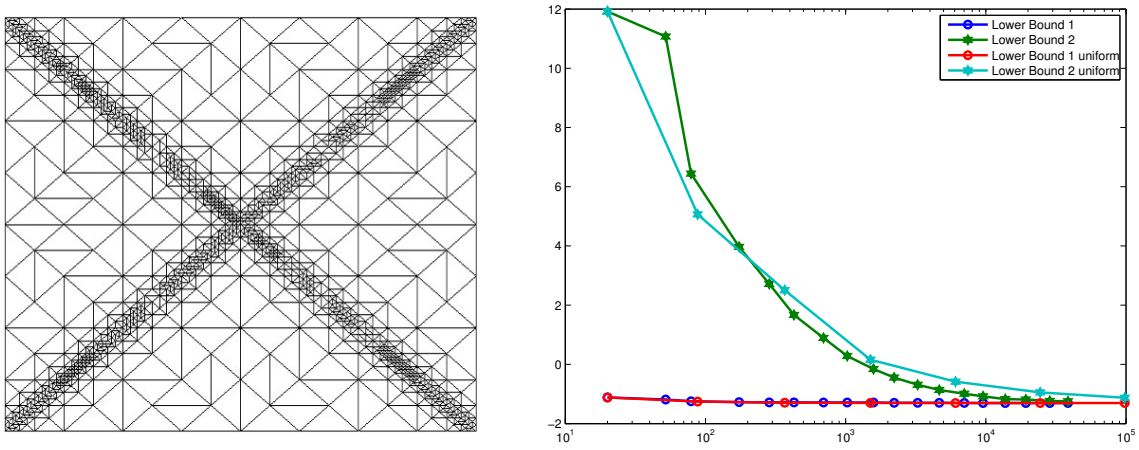

Figure 4.6: Adaptive mesh with refinement indicator η_{P1red} (left) and $E(u)-$lower bound for the lower bounds μ_1 and μ_2 of the exact energy $E(u)$ on uniform and adaptive meshes for Example 3.

[BS08] S. Brenner and L.R. Scott. *The Mathematical Theory of Finite Element Methods*. Springer, 2008.

[CGR12] Carsten Carstensen, Joscha Gedicke, and Donsub Rim. Explicit error estimates for courant, crouzeix-raviart and raviart- thomas finite element methods. *Jounal of Computational Mathematics*, 30(4):337–353, July 2012.

[CM10] C. Carstensen and C. Merdon. Estimator competition for Poisson problems. *J. Comput. Math.*, 28(3):309–330, 2010.

[CPS12] C. Carstensen, D. Peterseim, and M. Schedensack. Comparison results of finite element methods for the poisson model problem. *SIAM J. Numerical Analysis*, 50(6):2803–2823, 2012.

[Fal74] R Falk. Error estimates for the approximation of a class of variational inequalities. *Mathematics of Computation*, 28(128):963–971, October 1974.

[GK09] C. Gräser and R. Kornhuber. Multigrid methods for obstacle problems. *J. Comput. Math.*, 27(1):1–44, 2009.

[KS80] D. Kinderlehrer and G. Stampacchia. *An Introduction to Variational Inequalities and Their Applications*. Harcourt Brace Jovanovich, 1980.

[Vee01] A. Veeser. Efficient and reliable a posteriori error estimators for elliptic obstacle problems. *SIAM J. Numer. Anal.*, 39(1), 2001.

[Wan03] Lie-heng Wang. On the error estimate of nonconforming finite element approximation to the obstacle problem. *J. Comput. Math.*, 21(4):481–490, 2003.